Journal of Nuclear Materials 473 (2016) 167–177

Contents lists available at ScienceDirect

Journal of Nuclear Materials

journal homepage: www.elsevier.com/locate/jnucmat

Metallography and fuel cladding chemical interaction in fast flux test facility irradiated metallic U-10Zr MFF-3 and MFF-5 fuel pins

W.J. Carmack [a, *], H.M. Chichester [a], D.L. Porter [a], D.W. Wootan [b]

[a] Idaho National Laboratory, PO Box 1625, Idaho Falls, ID 83415, USA
[b] Pacific Northwest National Laboratory, PO Box 999, Richland, WA 99354, USA

HIGHLIGHTS

- Irradiation and post irradiation examination of full-length metallic fast reactor fuel.
- Fuel cladding chemical interaction formation in full-length metallic fast reactor fuel.
- Correlation of FCCI with temperature and burnup.
- Comparison of full-length reactor fuel performance with test reactor fuel performance.

ARTICLE INFO

Article history:
Received 2 October 2015
Received in revised form
6 February 2016
Accepted 10 February 2016
Available online 27 February 2016

Keywords:
Metallography
Fuel cladding chemical interaction
Irradiated fuel pins
MFF
FFTF

ABSTRACT

The Mechanistic Fuel Failure (MFF) series of metal fuel irradiations conducted in the Fast Flux Test Facility (FFTF) provides an important comparison between data generated in the Experimental Breeder Reactor (EBR-II) and that expected in a larger-scale fast reactor. The MFF fuel operated with a peak cladding temperature at the top of the fuel column, but developed peak burnup at the centerline of the core. This places the peak fuel temperature midway between the core center and the top of fuel, lower in the fuel column than in EBR-II experiments. Data from the MFF-3 and MFF-5 assemblies are most comparable to the data obtained from the EBR-II X447 experiment. The two X447 pin breaches were strongly influenced by fuel/cladding chemical interaction (FCCI) at the top of the fuel column. Post irradiation examination data from MFF-3 and MFF-5 are presented and compared to historical EBR-II data.

1. Introduction

Metallic fuel was selected for fueling many of the first fast spectrum reactors, including Experimental Breeder Reactors (EBR)-I and II in Idaho, the FERMI-I reactor in Michigan, and the Dounreay Fast Reactor (DFR) in the United Kingdom [14,8]. Metallic U-Pu-Zr alloys were the reference fuel for the United States Integral Fast Reactor (IFR) program [13]. The Fast Flux Test Facility (FFTF) reactor was in the process of qualifying metallic fuel (U-10Zr in HT9 cladding, Series III. b design) as a driver fuel just before it was shut down [10]. An extensive database on the performance of advanced metallic fuels was generated as a result of operating all of these reactors and the IFR program.

The Mechanistic Fuel Failure (MFF) series of metal fuel irradiations conducted in the FFTF provides an important potential comparison between data generated in EBR-II and that expected in a larger-scale fast reactor like FFTF. The as-built conditions of MFF-3 and MFF-5 were very similar [10] in that both contained 169 pins (6.86 mm diameter) in a ferritic-martensitic (HT9) duct. The HT9 clad and wire-wrapped fuel pins contained U-10Zr fuel, sodium bonded to the cladding. Both assemblies had an Inconel 600

Abbreviations: BOC, beginning of cycle; BOL, beginning of life; DFR, Dounreay fast reactor; EBR, experimental breeder reactor; EFPD, effective full power day; EOC, end of cycle; FCCI, fuel-cladding chemical interaction; FFTF, fast flux test facility; FMF, fuel manufacturing facility; GASR, gas assay sample and recharge; HFEF, hot fuel examination facility; IFR, integral fast reactor; HT9, ferritic-martensitic steel; ICP-MS, inductively coupled plasma mass spectrometry; MFF, mechanistic fuel failure; MOX, mixed uranium–plutonium oxide; PICT, peak inner cladding temperature; PF, peaking factor; PIE, post-irradiation examination; WHC, Westinghouse Hanford Company.

* Corresponding author. Idaho National Laboratory, PO Box 1625, MS 3840, Idaho Falls, ID 83415, USA.
E-mail addresses: jon.carmack@inl.gov (W.J. Carmack), heather.chichester@inl.gov (H.M. Chichester), douglas.porter@inl.gov (D.L. Porter), david.wootan@pnnl.gov (D.W. Wootan).

http://dx.doi.org/10.1016/j.jnucmat.2016.02.019
0022-3115/

lower reflector, no upper reflector, and no depleted uranium blanket, as had been employed in the first long-pin metal fuel experiment in FFTF, IFR-1 [11]. The MFF-5 test assembly was prototypic of a FFTF Series III. b driver fuel assembly. This design included a 10.2 cm longer plenum than MFF-3. To increase fuel pin plenum size, the MFF-5 assembly included a redesigned handling socket and lower shield assembly, which resulted in elevating the fuel pins four inches, thus increasing the plenum length relative to pins from MFF-3 but maintaining the same pin length and axial fuel position as that of the Series I and II metallic fuel driver assemblies in FFTF. The lower axial reflector was 6.4 cm long; its length was 16.5 cm in the MFF-3 pins.

The FFTF reactor had a core height of 91.4 cm (36 in.) and a chopped cosine neutron flux profile. This resulted in a core with peak cladding temperature at the top of the fuel column but with peak burnup near the midplane of the core. The peak fuel radial centerline temperature was midway between the core center and the top of fuel, lower in the fuel column than in the EBR-II X447 experiment. The MFF-3 and MFF-5 qualification assemblies operated in FFTF to >10 at% burnup, and performed very well with no cladding breaches. The MFF-3 assembly operated to 13.8 at% burnup with a peak pin inner cladding temperature of 643 °C at beginning of life (BOL), and the MFF-5 assembly operated to 10.1 at % burnup with a peak inner cladding temperature of 651 °C at BOL. All fuel pins contained tag gas identification modules. This can be compared to the two pin breaches experienced in X447 at approximately 10 at% burnup and peak inner cladding temperatures of 648 °C and 638 °C, respectively [9]. Post-irradiation examination (PIE) of a pin from MFF-3 and MFF-5 has been conducted to understand the performance differences in the pins from these two reactors operating at similar peak cladding temperatures, and to establish the extent of FCCI present, a known contributor to the X447 pin breaches.

FCCI formation in metallic fuel is strongly coupled to temperature and burnup. Higher burnup provides greater generation of fission products and higher temperature provides greater mobility and a stronger driving force for diffusion and migration of constituents to the fuel-cladding interface for reaction. Typically, due to the flux and power profile in EBR-II, peak burnup and peak fuel temperature both occur at the top of the fuel column. Because FFTF fuel pins are much longer than EBR-II fuel pins, the associated peak burnup and peak fuel temperature occurs below the top of the fuel column, typically between 0.5 and 0.75 ×/L. The fuel pin breaches reported by Ref. [9] for the X447 experiment were due to FCCI penetration of the cladding. FCCI formation data from the MFF-3 and MFF-5 experiments provide an important comparison between the two reactors and contribute to the understanding of FCCI formation mechanisms in metallic fuel.

1.1. As-built condition

The nominal design features of the MFF-3 and MFF-5 assemblies are provided in Table 1. The as-built conditions of MFF-3 and MFF-5 were very similar. Notable differences included a 1-cm fuel pin length difference and slightly higher plenum to fuel volume ratio in MFF-5 over MFF-3.

1.2. Irradiation conditions and performance history

MFF-3 began irradiation in Cycle 10C in core location 2404; MFF-5 began irradiation in Cycle 11B-1 in core location 1304. Fig. 1 shows the FFTF core map for Cycle 12B-1, indicating the locations of the MFF-3 and MFF-5 assemblies during irradiation. The assemblies were irradiated in these positions throughout their duration in FFTF. Table 2 shows the initial predicted test operating parameters for the MFF-3 and MFF-5 assemblies at the beginning of cycle (BOC) for the insertion cycle.

The peak linear power for each assembly was calculated by multiplying the assembly fission power, a factor accounting for the difference between the power deposited in the pin (fuel and cladding) and the fission power, and the radial and axial peaking factors. The pin energy deposition for the U–10Zr metallic fuel pins differs from the standard MOX ($(U, Pu)O_2$) fuel pins in FFTF because the U-235 enriched pins release less energy per fission than pins driven by Pu-239 fission and have a different overall composition due to the internal sodium and zirconium in the metallic fuel pins. The difference in pin energy deposition rates for these metallic fuel pins was accounted for in the calculated peak pin powers.

The total heat distribution for the FFTF core (including non-fueled components) was obtained by combining the local direct fission heat production with other nuclear heat sources, such as gamma ray absorption, charged particle reactions, and neutron scattering recoils. The energy produced from all of these sources was combined and adjusted so that the total was properly normalized for a recoverable heat energy of 291 MW at full power for Cycles 9 through 12 (previously 400 MW for Cycles 1 through 8).

Based on the deposited energy distribution and nominal sodium flow rates for each core component, the outlet temperature for each assembly was calculated at BOC and end of cycle (EOC). The assembly flow rates varied slightly from cycle to cycle as the core loadings changed. The assembly flows were based on a calculated core pressure drop at the total reactor flow rate of 7.59×10^6 kg/hr.

The assembly sub-channel flow temperatures were calculated using the SUPERENERGY thermal hydraulic code [15] and SIEX fuel performance code [15]. The SAFE code [5] was used to calculate the pin temperature axial distributions, including the fuel centerline, peak inner cladding temperatures, and the cladding wall temperatures.

The SUPERENERGY code is a sub-channel code designed specifically for hexagon shaped, wire-wrapped pin bundles and was used to calculate the FFTF core assembly mixed-mean outlet temperatures, the assembly sub-channel temperatures of all core assemblies, the core assembly duct wall temperatures, and the temperature of the reflector assembly coolant channels. The assembly mixed mean outlet temperatures were used as a basis for comparison to the FFTF above-core instrumentation data and to show that the core loading plans were in compliance with FFTF technical specifications prior to reactor operation. The sub-channel temperatures were used in design analyses of test pins, post-irradiation data correlation of test pins, and for lifetime analyses of driver fuel pins. The duct wall temperatures were used in the structural analyses of the individual assemblies and of the core restraint system. The flow field was described in terms of two correlated parameters, a sub-channel mixing parameter and a swirl flow parameter. These two parameters, along with the energy equation and a sub-channel flow split model, completely describe the temperature field in a pin bundle. The mixing parameters and flow split correlations were based on extensive experimental test data. The pin power distributions from the HEDPIN computer program [15] were used as part of the input in determining the sub-channel temperatures.

Normalized pin power distributions were calculated using HEDPIN based on interpolating the fission powers from the calculational mesh to the pin positions. The pin power distributions and sub-channel coolant temperatures were used to determine fuel pin temperature and power profiles using the SAFE computer code in a manner identical to that performed for the EBR-II X447 experiment fuel pins for each cycle. From this analysis, two pins were identified for detailed temperature and axial power distribution analysis, followed by full non-destructive and destructive PIE. Pin serial

Table 1
Nominal design features of MFF-3 and MFF-5 assemblies.

	MFF-3	MFF-5
Fuel Alloy Composition	U-10Zr	U-10Zr
Fuel Slug Diameter	4.98 mm (0.196-in.)	4.98 mm (0.196-in.)
Fuel Slug Length	91.44 cm (36-in.)	91.44 cm (36-in.)
Fuel Plenum Volume	28.9 cm^3 at 25 °C	31.5 cm^3 at 25 °C
Plenum to Fuel Volume Ratio	1.63	1.79
Cladding Material	HT9	HT9
Cladding Outer Diameter	6.86 mm (0.270-in.)	6.86 mm (0.270-in.)
Cladding Wall Thickness	0.559 mm (0.022-in.)	0.559 mm (0.022-in.)
Fuel Pin Length	238.1 cm (93.75-in.)	237.1 cm (93.35-in.)
Fuel Smeared Density	75%	75%
Fuel theoretical density	15.8 g/cm^3	15.8 g/cm^3
Fuel enrichment (wt.% U235)	32.4	31.0
Wire Wrap Dia./Pitch	1.35 mm/15.24 cm (0.0535-in./6-in.)	1.35 mm/23.37 cm (0.0535-in./9.2-in.)
Sodium volume	6.2 cm^3 at 25 °C	6.2 cm^3 at 25 °C
Sodium Fill Above Fuel	2.54 cm (1.0-in.)	2.54 cm (1.0-in.)
Axial Fuel Restrainer	None	None
Subassembly Type	HT-9	HT-9
Hex-can material – First	HT-9	HT-9
Hex-can material – Second	HT-9	HT-9
Maximum Pin Linear Power	613 W/cm (18.7 kW/ft)	557 W/cm (17 kW/ft)
Assembly Peak Inner Cladding Temperature (BOL)	643 °C	651 °C

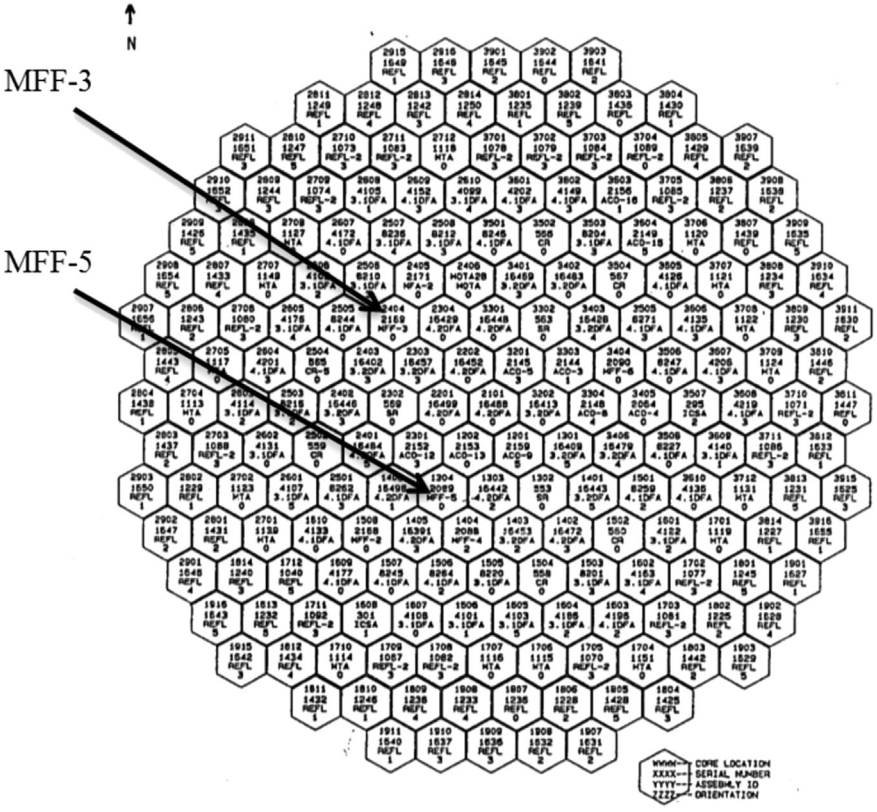

Fig. 1. FFTF Cycle 12B-1 core loading and positions of MFF-3 and MFF-5.

Table 2
Summary of MFF-3 and MFF-5 initial test operating conditions.

Test	Cycle	Core position	Calc T_{outlet} (°C)	Flow rate (kg/hr)	Flow rate (m^3/s)	Fission power (MW)	Axial PF	Radial PF	Peak Assembly Power (W/cm)
MFF-3[a]	B10C	2404	580	92210	113	7.867	1.24	1.066	608
MFF-5[a]	B11B1	1304	570	90881	112	7.360	1.21	1.058	553

[a] MFF-3 was irradiated for 726.2 effective full power days (EFPD); MFF-5 was irradiated for 503 EFPD.

number 193045 (a 4th row pin) from the MFF-3 assembly and pin serial number 195011 (a 4th row pin) from the MFF-5 assembly appeared to have experienced high power and, hence, high temperature operation, nearly peak for the assembly. Circles in Fig. 2 indicate the locations of Pins 193045 and 195011 in their assemblies. Fig. 3 provides a cycle-to-cycle history of the peak pin powers and the peak inner cladding temperatures for Pin 193045. Fig. 4 shows the axial linear power profile and axial temperature profiles for Pin 193045.

The analysis of the pin was conducted using the SAFE thermal analysis code. Particular attention should be called to the axial power profile and the extent to which it drops off in the upper half of the fuel column. As explained above, this causes the fuel pin centerline temperature to peak at a position lower in the relative axial height with respect to the top of the fuel column than that of the X447 (EBR-II) pins. This same behavior is also seen in MFF-5 Pin 195011. The cycle-to-cycle peak pin powers and peak inner cladding temperatures are shown in Fig. 5. The axial linear power profile and axial temperature profiles for Pin 195011 are shown in Fig. 6.

2. Results

2.1. Post-irradiation examination

Following completion of irradiation in 1994, non-destructive and destructive PIE of fuels from the MFF-3 and the MFF-5 assemblies have been performed, beginning in 2010. Pins 193045 and 195011 were subjected to neutron radiography, pin profilometry, gamma scan, fission gas sampling and analysis, metallography, micro-hardness, and isotopic chemical analysis to determine the extent of FCCI and the correlation with axial position, burnup, and operating temperature.

Following removal of pins from the assembly, no visible defects were observed. Neutron radiography and pin profilometry were completed and then the spiral spacer wire wraps were removed. Following removal of the spiral wraps, the pins were analyzed by axial gamma-ray spectroscopy (i.e., gamma-scanning). Destructive examination was initiated with pin puncturing and fission gas sampling and analysis. This was followed by sectioning, sampling, and polishing metallographic samples as well as burnup measurement. During metallographic examination, microhardness testing was also performed. Burnup samples were taken at locations adjacent to those selected for metallographic analysis and were analyzed by inductively coupled plasma mass spectrometry for isotopic and elemental composition determination.

2.1.1. Neutron radiography

Four irradiated metal fuel pins in each of MFF-3 and MFF-5 were radiographed using indium foil neutron detectors (epithermal neutrons) and dysprosium foil detectors (thermal neutrons). The activated foils were then used to transfer images to film. The films were ~43 cm long requiring six shots to cover the entire pin length of 240 cm.

The axial growth of the fuel slugs was measured using the neutron radiography, as shown in Fig. 7. A precision graduated (to 0.02 inches, or 0.51 mm) scale was placed next to the fuel during radiography and used to measure the fuel column length. The relative fuel column length changes are shown in Fig. 7 and are compared to a representative radiography of U–10Zr fuel (clad in D9, austenitic, stainless steel) previously irradiated in FFTF in assembly IFR-1 (Porter and Tsai, 2011). Note that the fuel in IFR-1 showed significantly greater axial growth and is much more similar to the experience gathered through EBR-II testing [6]. The IFR-1 peak cladding temperature (BOL) was 610 °C.

The measured fuel growth is shown in Table 3; the as-fabricated lengths are assumed from the specification (91.44 cm) as indicated in Fig. 7 as none were measured prior to irradiation.

Axial fuel column growth due to swelling is an important measurement in that most available metallic fuel column growth data is from 33.4-cm fuel column lengths of EBR-II experimental pins. A question as to whether cladding contact due to radial swelling restrains axial growth in full-length metallic fuel has existed due to the lack of full-length axial growth data. In addition, the aspect ratio is much larger for the FFTF fuel, creating more axial stress from the weight of the slug at the bottom of the fuel column. However, the fact that axial fuel growth observed in the IFR-1 experiment was only slightly less than EBR-II testing data indicates that there may be another factor involved in creating the low axial growth observations from MFF-3 and MFF-5. Additional studies are needed to fully understand this observation.

The HT9 cladding in the MFF experiments would have swollen much less than the IFR-1 D9, so one theory is that the axial strain of the cladding caused by void swelling may have induced more axial

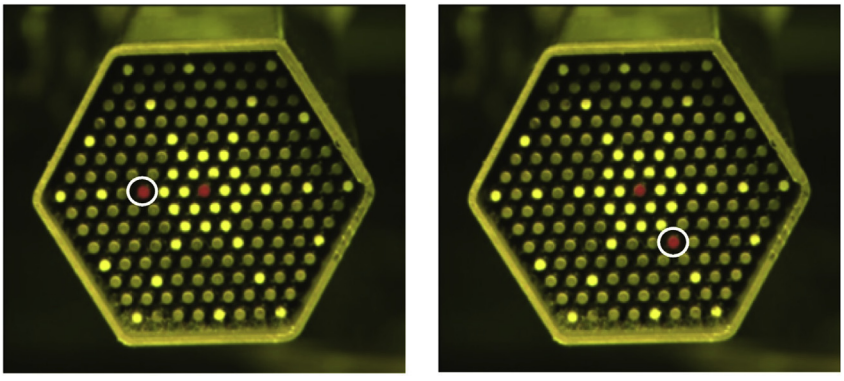

Pins selected from MFF-3 marked red. (locating notch positioned upper left corner.) White tipped pins retained for future testing.

Pins selected from MFF-5 marked red (locating notch positioned upper left corner.) White tipped pins retained for future testing.

Fig. 2. Photographs of the MFF-3 and MFF-5 assemblies following removal of the upper handling socket. Pins 193045 and 195011 have been marked along with the center pins for identification purposes.

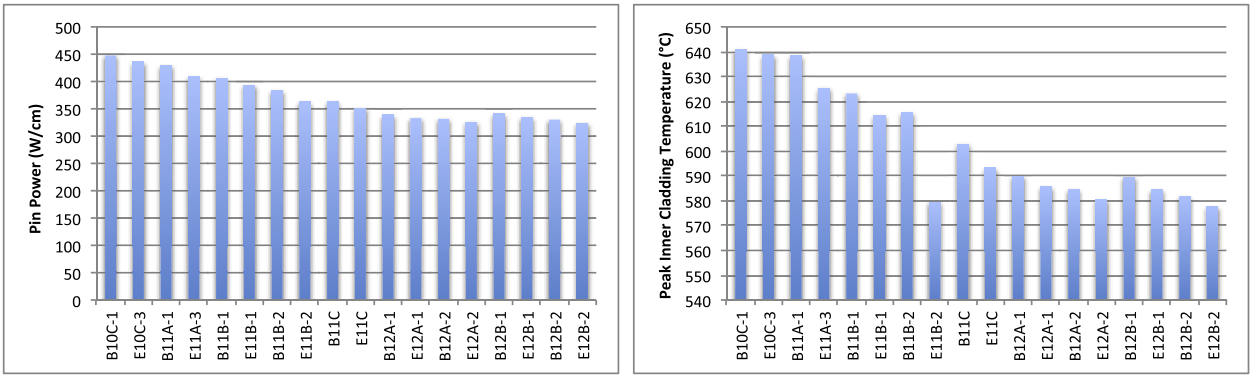

Fig. 3. MFF-3 cycle-to-cycle pin 193045 peak pin power (W/cm) and nominal peak inner cladding temperature (°C).

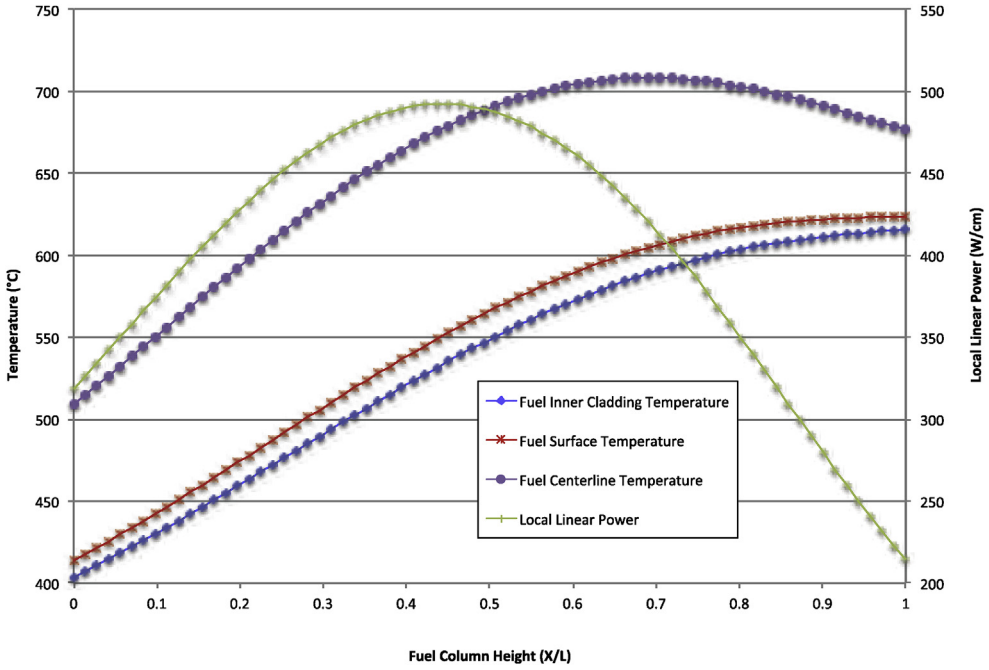

Fig. 4. Axial linear power and temperature profiles for MFF-3 Pin 193045. Values based on EFPD weighted values across all irradiation cycles.

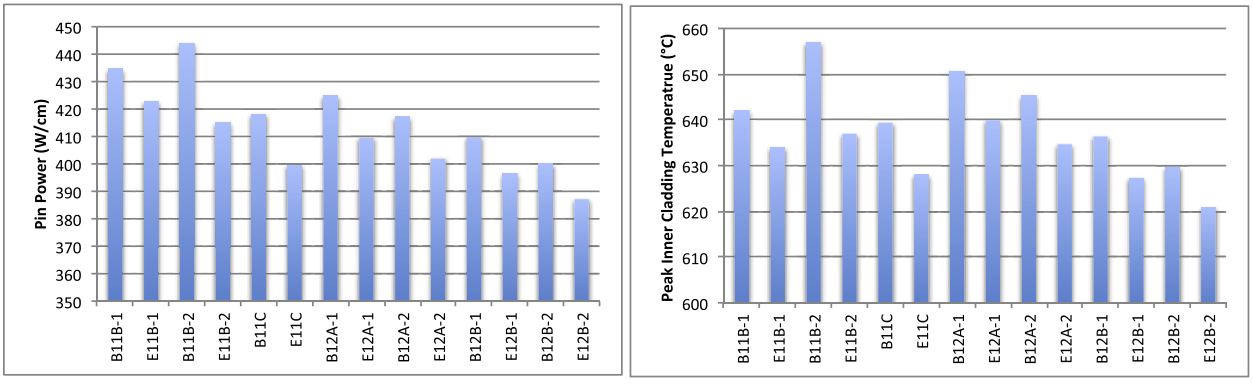

Fig. 5. MFF-5 cycle-to-cycle pin 195011 peak pin power (W/cm) and nominal peak inner cladding temperature (°C).

growth in the fuel. However, the swelling induced axial strain peaked at 3% in the core center [11]; therefore, averaged over the fuel column length, the strain would be much less than observed in the fuel column growth. The only other difference was the cooler operating temperature.

FFTF assemblies were each monitored for outlet temperature.

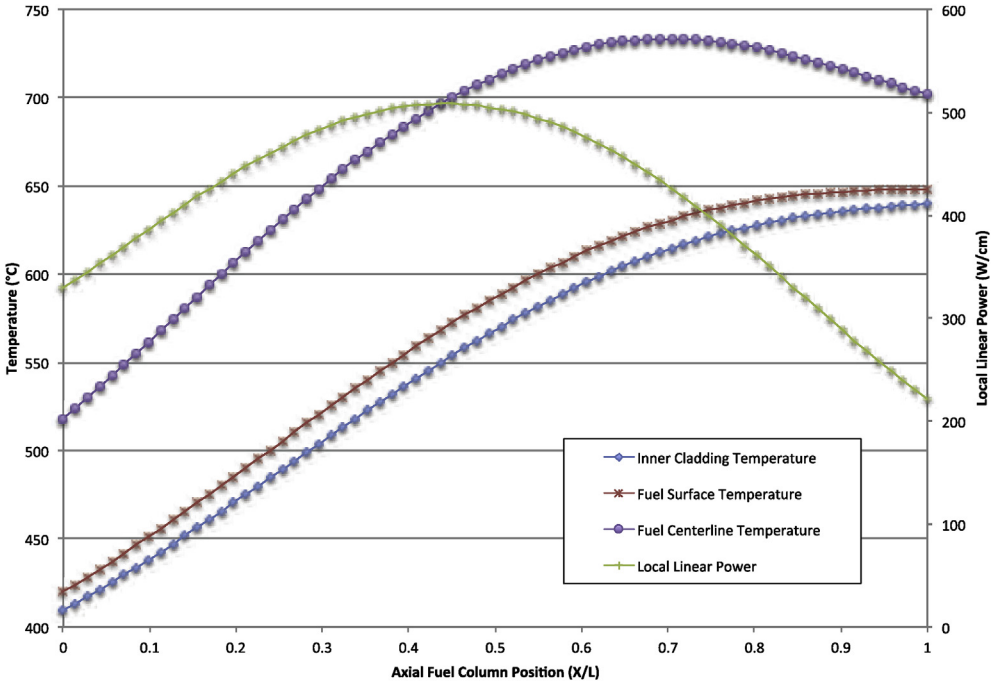

Fig. 6. Axial linear power and temperature profiles for MFF-5 Pin 195011. Values based on EFPD weighted values across all irradiation cycles.

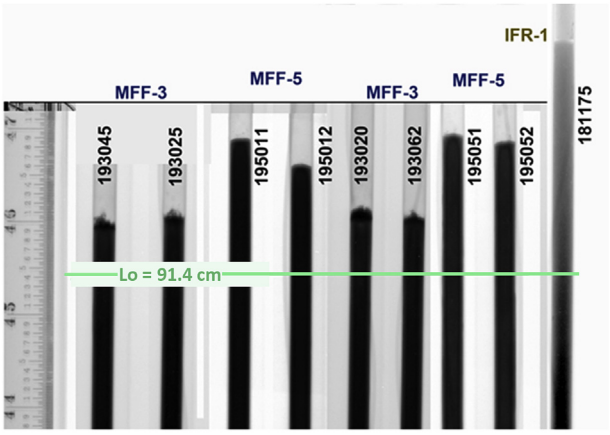

Fig. 7. Neutron radiography of the tops of the fuel columns of four MFF-3 and four MFF-5 pins, showing the low axial growth compared to a typical IFR-1 pin (36" = 91.4 cm, the initial fuel column length).

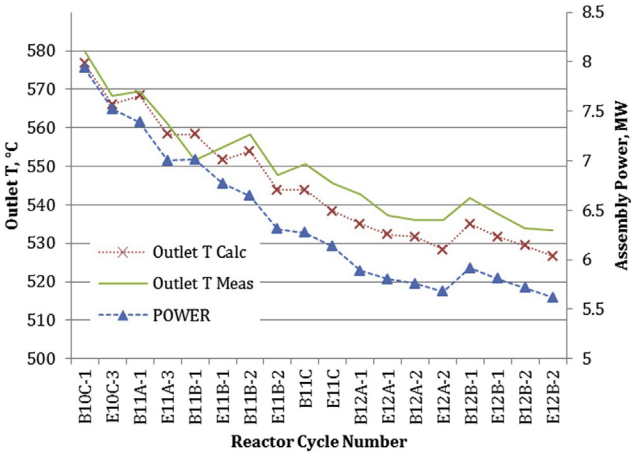

Fig. 8. MFF-3 Assembly power and outlet temperature (calculated and measured) at BOC and/or EOC.

Table 3
Axial growth of active fuel column as determined by neutron radiography.

	MFF-3				MFF-5			
Pin No.	193045	193025	193020	193062	195011	195012	195051	195052
$\Delta L/L_o$, %	1.5	1.6	1.8	1.6	3.7	3.0	3.9	3.8
Avg., %		1.6				3.6		

The previously conducted irradiation of the MFF-2 assembly exhibited a decline in outlet temperature that was larger than could be explained by depletion of fissile material content. A graphical representation of this is shown in Ref. [3]. A similar phenomenon was seen in the outlet temperatures of the IFR-1 assembly [2].

Assembly power and outlet temperature data are shown for MFF-3 in Fig. 8 and for MFF-5 in Fig. 9. Neither shows an under-prediction of the outlet temperature decline. This may be because the axial fuel growth experienced was small. The expansion of the fuel column of the U–10Zr fuel in the IFR-1 assembly was ~7%, at least twice that of MFF-3 and MFF-5. The MFF-2 axial expansion is to be measured in the future to test this theory.

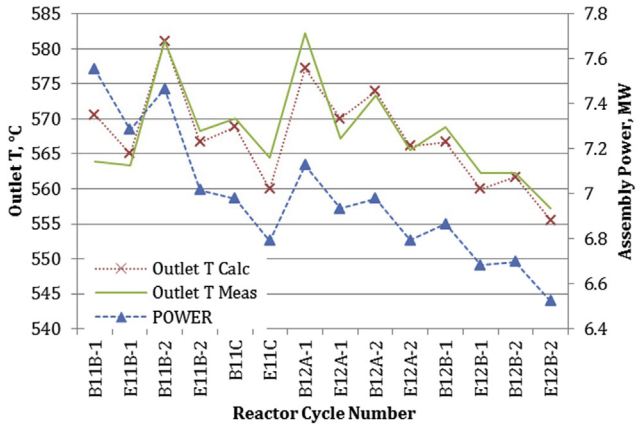

Fig. 9. MFF-5 Assembly power and outlet temperature (calculated and measured) at BOC and/or EOC.

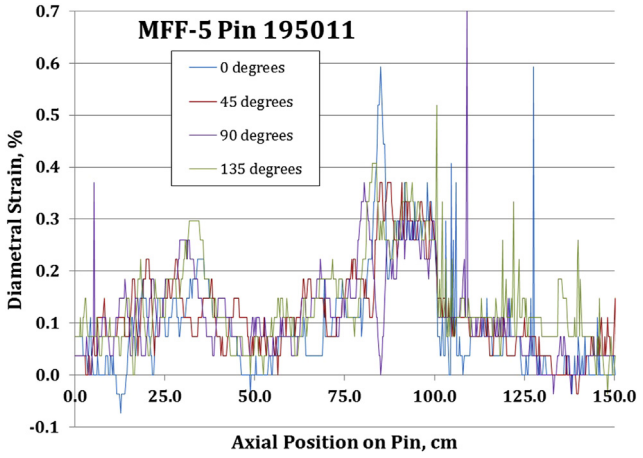

Fig. 10. Profilometry analysis of MFF-5 – 195011. Linear profilometry with rotations of the pin every 45°.

2.1.2. Cladding diameter (profilometry)

Fig. 10 provides the results of a linear profilometry scan of the 195011 fuel pin. This analysis indicates that a peak strain of 0.5% was developed over the course of the irradiation of the fuel pin. Peaks and valleys of strain coincident at 90° rotation indicates ovality (see 0° and 90° rotations at 85 cm elevation) perhaps caused by pinch lines where the bundle constricts on aligned wires.

Similar to Fig. 10, Fig. 11 provides a profilometry scan of the 193045 fuel pin indicating that a peak strain of 1.3% was experienced. The higher strain is expected in 193045 due to the higher burnup and neutron exposure of the assembly. While the peak at the top of the fuel column is likely temperature related (thermal creep) the other is likely generated by radiation induced creep or even void swelling. The axial location of peak power indicates the diameter peak lower in fuel column is not the location of highest exposure. However, swelling in HT9 appears to peak at 400–450 °C [4,12]. These temperatures are predicted to occur even lower on the pin than the peak location; further microstructural examination of the cladding may be needed to identify any partitioning between creep and swelling.

2.1.3. Precision gamma scanning

Eight pins, four from MFF-3 and four from MFF-5, were scanned axially for gamma radiation. Parameters used were a slit width of 2.54 mm, step size of 2.54 mm, and a live time of 240 s. Cs-134, Co-60 and Eu-154 isotopes were the only long-lived fission and activation products that could reliably be scanned. The Co-60 would mark the stainless steel (HT9) hardware locations. The Cs-134 represents the very mobile fission products that form a solution with the bond sodium and can therefore identify the location of sodium in the fuel pin plenum above the fuel column. The Eu-154 was the only rare earth fission product remaining that could be scanned. There were no relatively immobile fission products remaining to assess were the fuel was located. The gross activity (all isotopes) was also recorded.

Fig. 12 shows a typical gamma scan trace for MFF-3 pin 193045. The Co-60 traces show where the activated stainless steel (HT-9) from the fuel jacket and end plugs is located, and especially the Inconel reflector. The Cs-134 is peaked in the typical region just above the fuel where Cs gets trapped in the bond sodium that forms a molten plug above the fuel column. Some of these plugs can be forced upwards by build-up of fission gas in the plenum, although there are no obvious spikes in Cs shown here. Fig. 13 shows a typical gamma scan trace for the MFF-5 fuel pin 195011.

Supported by neutron radiography for MFF-3 and MFF-5, and the Cs-137 trace, the sodium on top of the fuel column is observed. There is also a small amount of sodium found at the bottom of the fuel column. The Co-60 signal can be attributed to steel components of the fuel pin. The large signal at the bottom of the fuel pin coincides with the lower Inconel reflector used to position the fuel

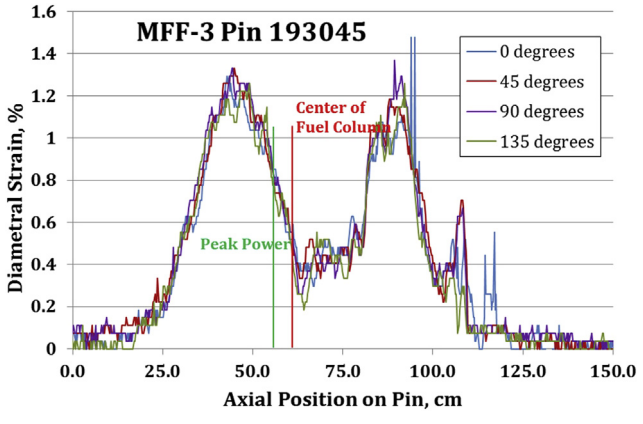

Fig. 11. Profilometry analysis of MFF-3 – 193045. Linear profilometry at 45-degree rotations of the pin.

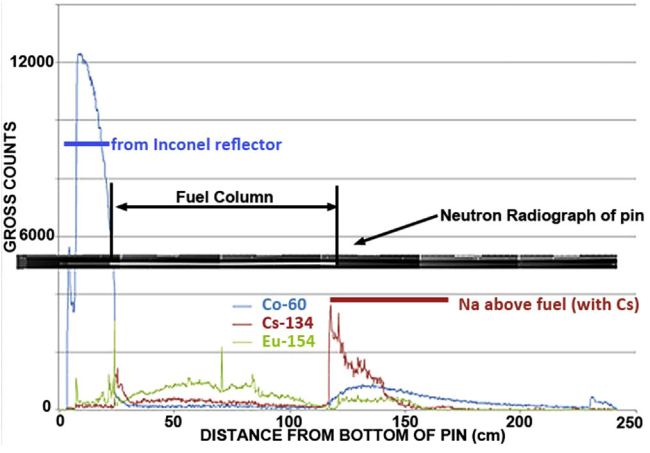

Fig. 12. MFF-3 Pin 193045 Neutron Radiography superimposed on gamma scan.

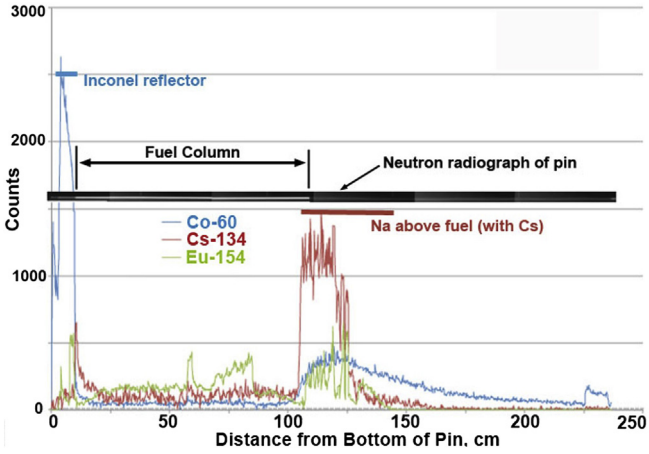

Fig. 13. MFF-5 Pin 195011 Neutron Radiography superimposed on gamma scan.

column with respect to the FFTF reactor core. The Eu-154 is a fission product that is usually used to indicate relative burnup in the fuel, but in the case of these two pins, most of the Eu-154 has decayed to the point that the signal is not useful for burnup analysis.

2.1.4. Fission gas release

The gas assay sample and recharge (GASR) system provides the ability to puncture cylindrical capsules or fuel elements to measure the free volume and pressure and to gather a sample for gas composition and isotopic analyses. With the sampling head secured to the fuel pin cladding, a laser penetrates the cladding wall under the sampling head. The sampler is positioned on the gas plenum region of the fuel pin, and when punctured the fission gas in the plenum is released to the GASR system. It is collected into a known volume and the pressure is measured. This provides a measure of the total gas in the plenum. A gas sample is taken to measure composition using a gas mass spectrometer. Finally, the fuel pin plenum is backfilled to measure its volume, thus providing a way to calculate the gas pressure that existed in the fuel plenum.

Table 4 provides a predicted amount of fission gas produced during irradiation. It also shows plenum volumes and the pressure and moles of fission gas collected during GASR testing. Based upon these numbers, the final row of the table shows the percentage of gas released. Note that the two U–10Zr pins punctured from the IFR-1 experiment showed gas release of 69% and 73%; so in comparison, the MFF-3 data looks low and the MFF-5 looks high. It appears that a larger data set is required to relate design or operating parameters to gas release.

Note that the gas release percentages of 61% and 79% are below but comparable to release percentages for either EBR-II sized pin irradiations or the IFR-1 FFTF metal fuel tests [11].

Table 4
Fission gas pressure and volume measured for MFF-3 and MFF-5 fuel pins.

Test number	MFF-3	MFF-5
Pin Number	193045	195011
Fuel Type	U-10Zr	U-10Zr
Avg Fission density, $10^{21}/cm^3$	4.3	3.1
Peak BU (a/o)	13.8	10.1
Avg BU (a/o)	10.85	7.61
Fuel Mass, g[a]	281.3	281.3
Fuel Volume (cm^3)[a]	17.8	17.8
Moles of HM burned	0.116	0.081
F.G. generated (moles)	0.0314	0.0233
Plenum Pressure (psi)[b]	322.4	272.3
Plenum Volume (cm^3)[b]	21.7	24.8
Moles Gas in plenum	0.0190	0.0184
Fission Gas Release, %	61	79

[a] Design.
[b] Measured (GASR).

2.1.5. Metallography

Metallographic sections and burnup samples were taken from five axial locations in both the 193045 and 195011 fuel pins. The locations specified included the 0.03, 0.25, 0.5, 0.75, and 0.96 ×/L locations corresponding to a sample from the top and bottom of the fuel column, and three additional evenly spaced locations, including a sample from the middle of the fuel column. The metallography of pins 193045 and 195011 was as expected for U–10Zr metallic alloy fuel irradiated to these burnups. Restructuring of the fuel microstructure experienced in the MFF experiments is typical of U–10Zr metallic alloy fuel. Figs. 14 and 15 summarize the results of metallographic analysis of the 193045 and 195011 fuel pins. The local average burnup determined by inductively coupled plasma mass spectroscopy (ICP-MS) analysis, the EFPD averaged peak inner cladding temperature, and the observed FCCI thickness are also summarized. Detail metallographic results and photomicrographs for the MFF-3 and MFF-5 fuel pins are available in Appendix E of [1].

Fig. 16 is a 100× optical photomicrograph of a high FCCI region of the MFF-3 193045 fuel pin at the X/L = 0.98 axial location. The extent of FCCI can be clearly seen in this sample resulting in approximately 150 μm of interaction layer thickness. The diamond-shaped features are hardness test indents.

The experimental data obtained from the MFF-3 and MFF-5 fuel pins provide a measure of the formation of an FCCI layer at locations with lower temperatures than those found in the X447 (EBR-II) fuel pins, but with a broader range of burnups and exposure time. The MFF-3 experiment achieved significantly higher burnup than did the X447 experiment [9].

3. FCCI formation with burnup and temperature

A key factor determining the operational lifetime, power, and temperature capability of metallic fuel is the formation of FCCI as it weakens the cladding (forms a brittle, fragile layer) and ultimately contributes to cladding failure. FCCI is dependent upon the production of lanthanide fission products in the fuel during the irradiation process and the migration of these species to the fuel-cladding interface for reaction/interaction with cladding constituents. The FCCI layer includes all reaction formation at the fuel cladding interface. The migration of the lanthanide and fuel constituent species are strongly tied to temperature. Previous experimental studies of FCCI indicate a correlation between FCCI formation and fuel operating temperature and burnup [7]. Keiser [7] provides summaries of the element trace analyses performed on a variety of metallic fuel and cladding combinations irradiated in EBR-II. Keiser identified phase formation on both sides of the fuel-cladding interface. Iron and nickel were found to diffuse into the fuel from the cladding and fuel constituents including lanthanides were found to diffuse into the cladding. It was found that lanthanide series species penetrated deepest into the cladding. Table 5 provides a summary of data taken from the previous X447 experiments and the MFF-3, and MFF-5 experiments of this study. The data indicates the axial location of measurements from the bottom of the fuel column. Local burnup is calculated by scaling the reported cycle-to-cycle pin average burnup to the normalized pin power profile for each cycle. Calculated, EFPD averaged inner cladding and fuel centerline temperatures are also reported.

The data show a relationship to burnup, fuel centerline temperature, and the peak inner cladding temperature. The FCCI

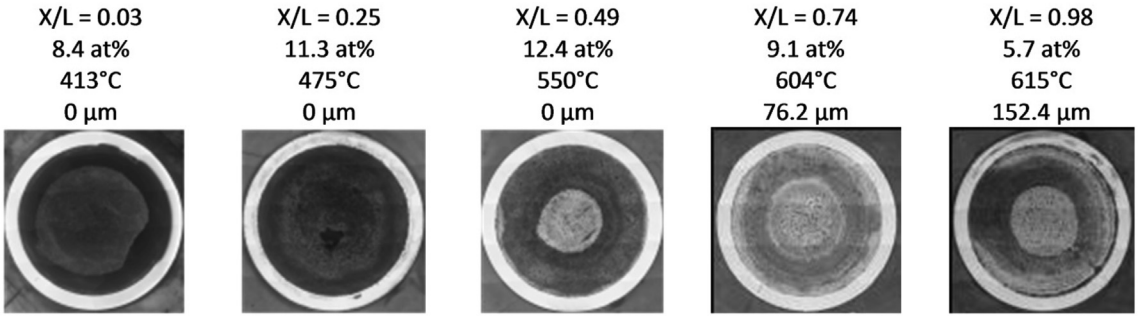

Fig. 14. Gross metallography of the MFF-3 pin 193045 showing microstructure along the axial length of the fuel column.

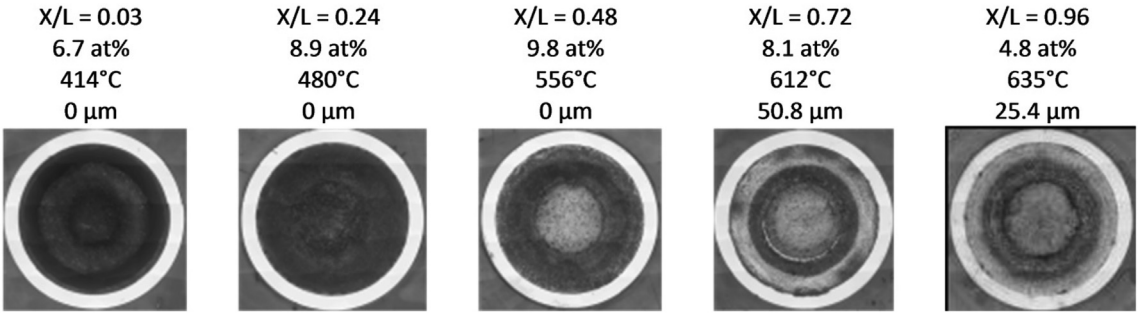

Fig. 15. Gross metallography of the MFF-5 pin 195011 showing microstructure along the axial length of the fuel column.

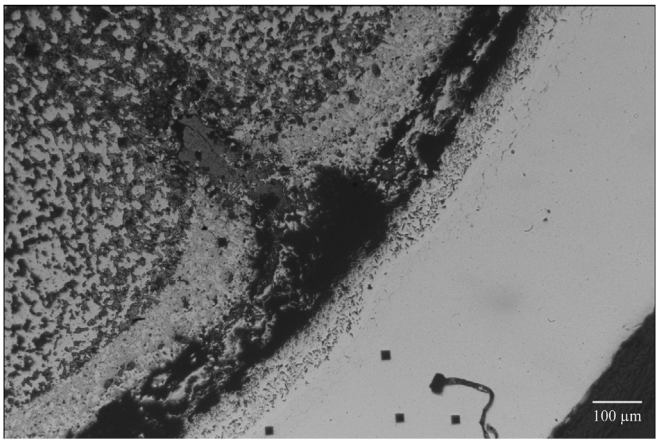

Fig. 16. Optical photomicrograph of high FCCI region of MFF-3 Pin 193045 at X/L = 0.98 – Sample 83T.

formed in the EBR-II X447 fuel pins peaks near the top of the fuel column [9]. This is because lanthanide fission product generation is high at this point, and the temperature at the fuel-cladding interface is highest at this point. The fuel centerline temperature is also high at this location and near its peak in most cases.

The differences between power profile and resulting temperature profile can be immediately seen. The power profile is shown to peak lower in the fuel column relative to the top of the fuel, and the fuel temperatures begin to drop before reaching the top of the fuel column. This is especially true in the case of the fuel centerline temperature. FCCI is lower than that found in the X447 fuel pins when compared at similar burnups. The MFF-3 fuel pin operated to a peak burnup of 13.8 at% and operated with a fuel centerline temperature that peaks at 710 °C at a fuel height of X/L = 0.7, dropping off to a fuel centerline temperature of 675 °C at the top of the fuel column. It is important to note that although the data collected on the MFF-3 pin did not show a pronounced drop in FCCI at the top of the fuel column, it is apparent that the FCCI in the pin is much lower than that experienced in the X447 experiments in EBR-II, see Table 4.

The MFF-5 assembly reached 10 at% burnup and operated at similar temperatures to those found in the X447 experiment, namely, fuel centerline temperatures near 700 °C and PICT near 650 °C. But the FCCI layer was much thinner than that in the X447 pins, peaked at a fuel column location of X/L = 0.7 (50 μm), and dropped to 25 μm at the top of the fuel column. This is similar to the behavior observed by Ref. [11] for the U-Pu-Zr based fuel in the IFR-1 experiment.

Extensive reconstruction of the operating conditions was performed to accompany the examination, providing detailed operating conditions axially along the pins. In addition, detailed ORIGEN calculations provided fuel burnup along the pin length. These calculations and detailed cross-section metallography allowed a Ph.D. dissertation to be conducted where the FCCI was modeled using Fickian and Soret effect-driven diffusion and interaction of rare earth fission products to the cladding surface [1].

An interesting feature observed and explained analytically by Ref. [11] is that an increasing Ce-144 activity near the top of the fuel column is observed as Ce migrates radially from the interior of the fuel slug to the outer surface of the fuel, resulting in higher gamma scanning signature for Ce-144. The Ce-144 signal has less self-shielding from the fuel as it migrates from the interior of the fuel pin and collects as a fuel-cladding interaction product on the inner diameter of the cladding. This is not seen in the gamma scanning data collected on the MFF-3 and MFF-5 fuel pins because by the time gamma scanning was conducted on MFF-3 and MFF-5, the Ce-144 lanthanide fission product had decayed away below the detectable limit of the gamma scanning instrument.

Table 5
Summary of FCCI data from X447[a], MFF-3, and MFF-5.

S/A	X/L0	Burnup (at%)	Fission density (fission/m^3)	Height from BOF (cm)	Measured max FCCI depth (μm)	Calculated time ave. fuel centerline temperature (°C)	Calculated time ave. cladding inner temperature (°C)
X447	**0.19**	**4.8**	1.70E+21	7	0	**574**	**463**
DP69	**0.46**	**7.9**	1.73E+21	17.1	0	**661**	**552**
	0.74	**4.1**	1.45E+21	25.4	51	**713**	**626**
	0.85	**3.5**	1.22E-21	29.2	51	**720**	**648**
	0.95	**2.7**	9.45E+20	32.4	102	**720**	**664**
	1	**2.4**	8.59E+20	34.3	102	**718**	**667**
X447	**0.69**	**9.2**	3.27E+21	24.8	64	**693**	**606**
DP04	**0.86**	**7.5**	2.65E+21	30.7	114	**704**	**634**
	0.94	**6.4**	2.26E+21	34.5	127	**705**	**644**
	0.95	**5.9**	2.09E+21	34.3	152	**704**	**649**
	0.97	**5.8**	2.05E+21	34.9	152	**703**	**649**
	0.98	**5.6**	1.98E+21	35.6	140	**703**	**650**
	1	**5.3**	1.87E+21	36.2	152	**701**	**652**
X447	**0.18**	**10.2**	3.61E+21	7	0	**563**	**457**
DP70	**0.49**	**10.6**	3.75E+21	17.1	0	**648**	**543**
	0.62	**9.9**	3.50E+21	22.9	28	**677**	**582**
	0.71	**9.3**	3.29E+21	25.4	25	**688**	**599**
	0.84	**7.7**	2.72E+21	30.7	86	**700**	**628**
	0.92	**6.8**	2.40E+21	33.7	117	**702**	**639**
	0.94	**6.5**	2.30E+21	34.3	97	**702**	**641**
	0.95	**6.3**	2.23E+21	34.9	91	**702**	**643**
	0.97	**6.1**	2.16E+21	35.6	127	**701**	**644**
	0.98	**5.9**	2.09E+21	36.2	140	**701**	**645**
	1	**5.7**	2.01E+21	36.8	89	**700**	**647**
X447	**0.19**	**10.2**	3.61E+21	7	0	**581**	**457**
DP75	**0.44**	**10.7**	3.78E+21	17.1	13	**659**	**533**
	0.68	**9.5**	3.36E+21	25.4	13	**707**	**596**
	0.81	**8.2**	2.90E+21	30.5	64	**721**	**622**
	0.9	**7.3**	2.58E+21	33.7	127	**724**	**635**
	0.91	**7**	2.47E+21	34.3	127	**724**	**637**
	0.93	**6.8**	2.40E+21	34.9	133	**725**	**640**
	0.94	**6.5**	2.30E+21	35.6	140	**724**	**642**
	0.96	**6.3**	2.23E+21	36.1	146	**724**	**644**
	0.98	**5.9**	2.09E+21	36.8	152	**724**	**646**
MFF5	**0.03**	**6.7**	2.37E+21	2.5	0	**532**	**414**
195011	**0.24**	**8.9**	3.15E+21	22.9	0	**628**	**480**
	0.48	**9.8**	3.46E+21	45.7	0	**712**	**556**
	0.72	**8.1**	2.86E+21	68.6	51	**736**	**612**
	0.96	**4.8**	1.70E+21	91.4	25	**709**	**635**
MFF3	**0.03**	**8.4**	2.97E+21	2.5	0	**527**	**413**
193045	**0.25**	**11.3**	3.99E+21	22.9	0	**619**	**475**
	0.49	**12.4**	4.38E+21	45.7	0	**700**	**550**
	0.74	**9.1**	3.22E+21	68.5	76	**712**	**604**
	0.98	**5.7**	2.01E+21	91.4	152	**682**	**615**

Note: Calculated temperatures are EFPD averaged over the irradiation cycle histories.
[a] Data from X447 taken from Ref. [9].

The data shown in Ref. [11] confirms this finding. Porter and Tsai report the FCCI layer thickness across the axial fuel column measured during optical metallography examination. The data show that the FCCI peaks near the peak of the axial power profile and reduces back to zero at the top of the fuel column.

4. Summary and conclusions

The MFF series of metallic fuel tests performed in the FFTF were the beginning tests to qualify U-10wt%Zr as a driver fuel for FFTF. The fuel pins all performed very well to relatively high burnup and with no pin breaches. Tests MFF-3 and MFF-5 were chosen to be destructively examined because they were run at high peak cladding temperatures (615 °C and 635 °C, respectively) and to significant burnup (138 and 101 MW d/kgM, respectively). They were the only sodium fast reactor metallic fuel tests with long (91.4 cm) fuel columns and clad in HT9 to be operated at these high temperatures.

The examination of the MFF-3 and MFF-5 pins included neutron radiography, axial profilometry including pin bow and length measurements, precision gamma scanning, plenum gas puncturing to measure fission gas release, detailed chemical/isotopic analyses of fuel samples to confirm burnup calculations, and metallography of pin cross-sections. The PIE conducted on the MFF-3 and MFF-5 assemblies produced several interesting findings.

1 The axial fuel growth was very small, only 1.7% and 3.6% for MFF-3 and MFF-5, respectively, compared to the earlier FFTF tests where U–10Zr fuel swelled axially ~7%. Comparing design and operating conditions, the high operating temperature of the MFF-3 and MFF-5 tests are suspected as the potential cause. This is an important finding for predicting future sodium-cooled fast reactor fuel pin designs.
2 The axial profilometry of the higher burnup MFF-3 pin (19×10^{22} n/cm^2, E > 0.1 MeV) showed a pronounced double peak, one at the top of the fuel column and the other a little below peak flux location on the fuel column. MOX pins have previously shown this behavior with HT9 cladding. This may be due to a peaking in thermal creep at the top due to high cladding temperature, some wall thinning due to FCCI, and a peaking of the irradiation creep further down the fuel column due to high

neutron exposure. Fuel pin length measurements indicated there may also be cladding swelling, but there was too much apparent growth in the MFF-5 pins to be accounted for with the small diameter increases. Cladding density would need to be confirmed.

3 The fission gas release value was low (61%) for MFF-3 compared with other test results, including MFF-5 (79%). However, only one pin from each test was measured and more testing would be needed to see a statistically relevant trend.

4 FCCI formation is clearly dependent upon burnup and temperature. Data indicates that longer length fuel having peak burnup at lower temperatures appears to reduce the rate of formation of FCCI along the fuel column. Additional data is needed to fully explain the transport mechanism responsible for diffusion of fuel and cladding constituents in metallic alloy fuels.

5 Other pin performance characteristics looked very much like that exhibited by the fuel tests previously performed in the EBR-II on much shorter pins. Metallography and other exams were consistent with the results from other tests, including the large database collected from tests performed on shorter pins in EBR-II.

Future work could include further study of gas release using other MFF pins, including the colder operating pins from MFF-2 and/or MFF-6. Likewise, the axial fuel growth could be further examined for links to operating temperature by producing neutron radiographs of pins from MFF-2 and MFF-5.

Disclosure statement

Role of funding source

The funding source had no role in the research or writing of this paper, or the decision to submit it for publication.

Acknowledgments

The authors would like to thank all of those who made these experiments possible, including the skilled craftsmen in the INL Fuel Manufacturing Facility (FMF), who fabricated the fuel slugs; those at the Hanford Westinghouse Hanford Company (WHC), who fabricated the fuel pins and experiment assemblies; Ron Baker, who led the effort to qualify U–10Zr metallic fuel for use in FFTF, supported by Jim Dittmer (fabrication), MFF experimenter Al Pitner, and others; and the WHC analysts whose calculations guided reactor placement and flow to produce the right operating conditions and provided the safety analysis to establish a basis for the experiments to be irradiated. Jim Corrigan led this team of analysts, which included A. E. Bridges and others.

The authors would also like to thank all those who performed expert characterization of the as-irradiated pins in the Hot Fuel Examination Facility (HFEF) and the Analytical Laboratory at the INL Materials and Fuels Complex. HFEF engineers Glen Papaioannou, Paul Lind, Katelyn Wachs, and David Sell are especially to be thanked.

References

[1] W.J. Carmack, Temperature and Burnup Correlated FCCI in U-10Zr Metallic Fuel, Ph.D. dissertation, University of Idaho, 2012 (May).
[2] E.R. Cramer, A.L. Pitner, In Situ Observation of Axial Irradiation Growth in Liquid-metal Reactor Metal Fuel 60, Transactions of the American Nuclear Society, San Francisco, CA, 1989, pp. 306–307.
[3] Ethridge, J.L. to Seidel, B.R., 1988. MFF-2 Axial Fuel Growth to Account for Power Decrease. Personal Communication, September 12.
[4] Garner, F.A., Toloczko, M.B., 1995. Irradiation creep and swelling of two LMR heats of HT9. Fusion Materials Semiannual Progress Report for the Period Ending March 31, 1995. DOE/ER-0313/18, 169–178.
[5] S.L. Hayes, SAFE: a Computer Code for the Steady State and Transient Thermal Analysis of LMR Fuel Elements, 1993. Argonne National Laboratory Report. ANL-IFR-221, December.
[6] G.L. Hofman, R.G. Pahl, C.E. Lahm, D.L. Porter, Swelling behavior of U-Pu-Zr fuel, Metall. Trans. A 21A (1990) 518–528.
[7] D.D. Keiser, The development of FCCI zones in irradiated U-ZR and U-Pu-Zr fuel elements with stainless steel cladding, in: A. Aasen, P. Olsson (Eds.), Nuclear Reactors, Nuclear Fusion and Fusion Engineering, Nova Science Publishers, Inc., Hauppauge, NY, 2009. ISBN: 978-1606925089.
[8] J.H. Kittel, B.R.T. Frost, J.P. Mustellier, K.Q. Bagley, G.C. Crittenden, J. Van Dievoet, History of fast reactor fuel development, J. Nucl. Mater. 204 (1993) 1–13.
[9] R.G. Pahl, C.E. Lahm, S.L. Hayes, Performance of HT9 clad metallic fuel at high temperatures, J. Nucl. Mater. 204 (1993) 141–147.
[10] A.L. Pitner, R.B. Baker, Metallic fuel test program in the FFTF, J. Nucl. Mater. 204 (1993) 124–130.
[11] D.L. Porter, H. Tsai, Full-length U–xPu–10Zr (x = 0, 8, 19 wt.%) fast reactor fuel test in FFTF, J. Nucl. Mater. 427 (2012) 46–57.
[12] B.H. Sencer, J.R. Kennedy, J.I. Cole, S.A. Maloy, F.A. Garner, Microstructural analysis of an HT9 fuel assembly duct irradiated in FFTF to 155 dpa at 443 C, J. Nucl. Mater. 393 (2009) 235–241.
[13] C.E. Till, Y.I. Chang, Plentiful Energy: the Story of the Integral Fast Reactor: the Complex History of a Simple Reactor Technology, with Emphasis on its Scientific Bases for Non-specialists, CreateSpace Independent Publishing Platform, 2011. ISBN: 978-1466384606.
[14] L.C. Walters, B.R. Seidel, J.H. Kittel, Performance of metallic fuels and blankets in liquid-metal fast breeder-reactors, Nucl. Technol. 65 (1984) 179–231.
[15] Wootan, D.W., Nelson, J.V., 2012. Burnup predictions for metal fuel tests in the fast flux test facility. 2012 ANS Annual Meeting, Embedded Topical Meeting: Nuclear Fuels and Structural Materials for the Next Generation Nuclear Reactor. Chicago, IL, June 24–28.